DATA REPOSITORY

Did the great dying of life take 700 k.y.? Evidence from global astronomical correlation of the Permian-Triassic boundary interval

Huang et al.

Permo-Triassic boundary (PTB) sections at Shangsi, Meishan B, Huangzhishan (HZS), and Heping (HP) in South China and the Gartnerkofel-1 (GK) core in Austria were selected to study the PTB mass extinction interval (MEI) (Fig. 1). The PTB MEI defined for this study (based on Figure 2 of (Jin et al., 2000)) is constrained from the start of the *Neogondolella meishanensis* conodont zone or *Hindeodus latidentatus preparvus-Neogondolella meishanensis* conodont zone or *Otoceras /Hypophiceras* ammonoid zone at the onset of the negative $\delta^{13}C$ excursion (ME_{start}), to the base of the *Isarcicella isarcica* conodont zone or *Ophiceras* ammonoid zone and *Claraia wangi* bivalve assemblage zone and increasing $\delta^{13}C$ values (ME_{end}) (Fig. 1). Conodont zones and carbon isotope ($\delta^{13}C$) series from these five sections correlate well to one another (Fig. 1); $\delta^{13}C$ and magnetic susceptibility (MS) data from these sections are examined for the presence of correlated astronomical frequencies. At Shangsi and HZS, the stratigraphic resolution of the $\delta^{13}C$ data is lower than that of accompanying MS data (Fig. 1 A, C); we used the latter to ensure the highest possible resolution. At Meishan, $\delta^{13}C_{carb}$ data was collected at high resolution (average spacing of 0.67 cm) as a proxy for carbon cycling related to the extinctions (Jin et al., 2000). MS data at Meishan is also available, but at lower resolution (Fig. 1 B and Fig. DR4), so we analyzed $\delta^{13}C_{carb}$. At HP and GK, the $\delta^{13}C_{carb}$ series have similar profiles through the PTB interval. At HP, ultimately we analyzed $\delta^{13}C_{org}$, which was measured at higher resolution and covaries with $\delta^{13}C_{carb}$, indicating a common carbon source for both proxies (Krull et al., 2004). Detailed lithological and biostratigraphic

information on these sections and further discussion on astronomical tuning are given below.

1. Shangsi, Sichuan Province, China

Location and facies description. The Shangsi section, located at 32º 7' N and 105º 30' E in Guangyuan city, Sichuan Province, southwest China, was one of the candidates for the global stratotype section and point (GSSP) for the PTB (Lai et al., 1996; Li et al., 1986). In this section, the latest Permian Dalong Formation (Formation abbreviation as Fm. in Fig. 1) consists of dark grey, organic-rich micrites and cherty micrites with several volcanic ash beds in the topmost levels. The overlying Feixianguan Formation is comprised of thin-bedded, alternating mudstones and micritic or argillaceous limestones in its lower part, and lacks the cherty concretions and radiolarian-bearing lithologies characteristic of the upper Dalong Formation. The facies change in the transition from the latest Permian to earliest Triassic has been observed in many other marine sections throughout South China (Wignall et al., 1995).

The detailed lithology of the PTB interval is as follows. Bed 21 is 2.61 m thick, and consists of grey to dark grey, thin- to medium-bedded siliceous micrite intercalated with siliceous shale. Bed 22 is 1.78 m thick, and consists of dark grey, thin- to medium-bedded siliceous mudstone intercalated with cherty limestone. Bed 23 is 6 cm thick, and consists of yellowish brown to grayish green thin-bedded illite-montmorillonite claystone. Bed 24 is 59 cm thick, and consists of dark grey, thin- to medium-bedded cherty limestone intercalated with siliceous shale. Bed 25 is 15 cm thick, and consists of yellowish green to white illite- montmorillonite claystone with interbeds of greyish black marls at the top. Bed 26 is 25 cm thick, and is a dark grey, thin-bedded siliceous micrite. Bed 27a is 5 cm thick, and is a greyish black montmorillonite and illite claystone. Bed 27b is 6 cm thick, and is a “white clay” consisting of greyish white, irregular illite and montmorillonite claystone with volcaniclastics. Bed 27c is 4 cm thick, and is a “black clay” consisting of greyish black illite and montmorillonite bearing laminated claystone. Bed 28 consists of green-grey marls mixed with brown, laminated, organic-rich shales and micritic mudstones (Bed 28a: 16 cm thick, Bed 28b: 24 cm thick, Bed 28c: 64 cm thick, Bed 28d: 74 cm thick). The bivalve *Claraia wangi* occurs at 45 cm below the PTB

between Bed 28 and Bed 29. Bed 29 is 1.91 m thick, and consists of greenish illite and montmorillonite laminated claystone intercalated with siliceous shale and marl. Bed 30 is 1.8 m thick, and is a yellow-green laminated marl intercalated with micrite. *Hindeodus parvus* occurs in the upper part of this bed. Bed 31 is 2.69 m thick, and is a thin-bedded micrite interbedded with grey, laminated dolomitic limestone with organic-rich laminae of algal lamination at the top of this bed (Lai et al., 1996; Li et al., 1986).

The Shangsi section records continuous hemipelagic deposition during the PTB interval. A major environmental change at Shangsi occurs just before PTB, which is visible in the magnetic susceptibility **(**MS) data (Figs. 2 and DR1). The disappearance of chert (last seen in Bed 26) and radiolaria-bearing lithologies is characteristic of the transition from Dalong to Feixianguan Formation. There are also changes in the macrofauna and trace fossils. Peak benthic diversity and shallow water taxa indicate a shallowing event at the base of Bed 22. Subsequently, the same fauna are present but are much less abundant; the majority of benthic and pelagic faunal extinctions occur at the Bed 26/27 boundary (ME_{start}). Of the 47 species recorded in the upper Dalong Formation only 10 cross this boundary. From Bed 27 upward the absence of bioturbation and presence of pyritic laminae suggest anoxic oceanic conditions (Wignall et al., 1995).

Stratigraphic framework. The PTB at Shangsi is placed at the Bed 28b/28c boundary based on the first occurrence of *Hindeodus decrescens* (a comparable morphotype of *Hindeodus parvus* (Lai et al.1996)) and other index conodont species such as *Hindeodus eurypyge* and *Hindeodus changxingensis* that define the PTB beds at Meishan (Lai et al., 1996; Metcalfe et al., 2007; Nicoll et al., 2002), although true *H. parvus* occurs at a much higher horizon in this section. Like *H. parvus*, *I. isarcica* also occurs much later in Shangsi than it does in other sections with its FO at 7 m above the PTB (Lai et al., 1996). However, the FOs of the bivalve *Claraia wangi* and ammonoid *Ophiceras* spp. at 45 cm below the Bed 28d/29 boundary may mark the horizon of ME_{end} because their FOs are usually associated with the FO of the *Isarcicella isarcica* conodont zone and ME_{end} at Meishan and Huangzhishan (Chen et al., 2009; Yin et al., 2001). It should be noted that the bed numbers of the Shangsi and the Meishan sections are not the same. At Shangsi, the *H. parvus* zone is more than 1 m thick, compared with only 8 cm at Meishan (Fig. 1). In sum, the MEI at Shangsi is equivalent to the *Otoceras-Hypophiceras* ammonoid zone.

The $\delta^{13}C_{org}$ data has a negative excursion in the MEI that is similar to that at Meishan and the other sections. The entire MS series has 1-2 cm sample rate with an average 1.47 cm and was resampled to a 0.5 cm uniform sample rate for the time series analysis (Fig. DR4).

Magnetostratigraphy.

Magnetostratigraphy is a useful tool for global correlation, however, the duration of reversal cannot be determined a priori (Erwin, 2006). Early studies of magneto-stratigraphy at Shangsi indicate that there are at least six polarity chrons in the PTB interval (Heller et al., 1988; Steiner et al., 1989). Recent work on three composite sections at Shangsi identifies 8 polarity chrons, and that the PT boundary mass extinction occurs within a normal polarity chron immediately above (50 cm) a R-N polarity transition (Glen et al., 2009).

Magnetic susceptibility and lithology. The magnetic susceptibility (MS) data presented in this paper was measured by Hansen et al. (2000). MS is inversely related to carbonate content along the section, evident from relatively low MS in the carbonate-rich interval (Beds 21-24), and increased MS in the overlying clay and mudstone rich interval (Beds 25-30); MS starts decreasing again from Bed 30 upwards (Heller et al., 1988) (Fig. DR1). The majority of the Shangsi samples are weakly magnetic and have low initial magnetic susceptibilities due to very low concentrations of ferromagnetic minerals (Glen et al., 2009; Heller et al., 1988). The pure or siliceous limestones have low natural remanent magnetization (NRM) intensities. Marls, muddy limestones and mudstones have both higher NRM and higher magnetic susceptibilities, indicating that detrital input contributes ferromagnetic constituents to the sediment and higher MS (Heller et al., 1988). We conclude that higher MS values are correlated with higher detrital fluxes from terrestrial sources to the marine environment (Lean and McCave, 1998).

Additional notes on chronology. At Shangsi, the duration of the MEI is based on the definition of ME_{start} and ME_{end}. The duration of the MEI is 692 k.y. from 405-k.y. tuning and 600 k.y. from the adjusted U-Pb age tuned series (Fig. 2). This is based on ME_{start} placed at the base of Bed 27 (Wignall et al., 1995) and ME_{end} defined at 45 cm below the top of the Bed 28d. However, based on the character of the MS data, ME_{start} could be at the base of Bed 25; and based on the $\delta^{13}C$ excursion ME_{end} could be at the base of Bed

28d; in that case, an alternative estimate duration of 670 k.y. is indicated for the MEI, based on 100 k.y. tuning (Fig. 3A).

2. Meishan, Zhejiang Province, China

Location and facies description. The well-known Meishan section located at 31º 4' 55" N and 119º 42' 22.9" E, is situated in the town of Meishan, Changxin County, Zhejiang Province, China, and is the Global Stratotype Section and Point (GSSP) for the PTB (Yin et al., 2001). The Meishan B section was studied and its PTB interval consists of, from bottom to top, a 5-cm-thick (grayish white to grey) illite-montmorillonite clay (Bed 25), a 6-cm-thick clayish calcareous black shale bed (Bed 26), a 16-cm-thick argillaceous limestone-argillaceous dolomite (Bed 27), a 4-cm-thick illite-montmorillonite grayish green-yellow clay (Bed 28), and mudstone-dolomitic mudstone (Bed 29). The Meishan sequence was deposited in a platform ramp/slope setting.

Stratigraphic framework. The PTB interval, only 31 cm thick, indicates extremely reduced sedimentation, diagenesis, burrowing, and possible submarine erosion, non-deposition and/or dissolution, especially within Bed 27 (Cao and Shang, 1998; Cao and Zheng, 2009; Nicoll et al., 2002). The 'main' mass extinction (ME_{start}) occurs at the base of Bed 25 (Jin et al., 2000; Song et al., 2009; Xie et al., 2005) or possibly as much as 2 cm below the base (Kaiho et al., 2006; Kaiho et al., 2001), while the end of the mass extinction, sometimes termed 'epilogue' extinction (ME_{end}) is calibrated to Bed 28 (Song et al., 2009; Xie et al., 2005; Yin et al., 2007). $\delta^{13}C_{carb}$ data were sampled at 0.09 to 3.43 cm intervals, averaging 0.67 cm (Jin et al., 2000) and were resampled to a 0.1 cm uniform sample rate for the time series analysis in this study (Fig. DR4B). ME_{start} corresponds to the base of the *Hindeodus latidentatus preparvus-Clarkina meishanensis* conodont zone (Bed 25-Bed 27b), which is just below the most negative $\delta^{13}C$ excursion; the *H. parvus* zone occurs in Beds 27c-d; the *I. isarcica* zone is in Bed 28 (Yin et al., 2001). However, Jiang et al. (2007) placed the *H. parvus* zone only in Bed 27c, the *Isarcicella staeschei* zone in Beds 27d and 28, the base of the *I. isarcica* zone at the base of Bed 29. This reassigns ME_{end} to the top of Bed 28 (Fig. 1B).

Additional notes on chronology. At Meishan, the FO of *H. parvus* (base of Bed 27c) occurs 380 k.y. after ME_{start} (base of Bed 25) compared with the geochronologic estimate

of 500 ± 300 k.y. (Bowring et al., 1998). The 100-k.y. tuned estimate (Fig. 3B) shows that the sharp negative excursion of $\delta^{13}C$ in Bed 27a lasted 100 k.y., slightly less than the geochronologic estimate of 165 k.y. (Bowring et al., 1998). The $\delta^{13}C_{carb}$ 100-k.y. tuned series indicates an MEI duration of 700 k.y. with ME_{end} placed at the base of the *I. isarcica* zone (at the top of Bed 28 at Meishan A) (Jiang et al., 2007). Previously, *I. isarcica* was known only within Bed 28, and the base of the *I. isarcica* zone had been defined at the base of Bed 28 (Yin et al., 2001). This latter placement makes the MEI duration at Meishan ~100 k.y. shorter than the other five sections. This placement of ME_{end} in Meishan affects correlation with other sections. In sum, at Meishan there is an ambiguity of where precisely the base of the *I. isarcica* zone occurs, and thus, in the precise placement of ME_{end}. Song et al. (Song et al., 2009) report the disappearance of 32 of 34 foraminiferal species at the base of Bed 28, suggesting that ME_{end} should be placed above the base of Bed 28.

In addition, the high-resolution $\delta^{13}C_{carb}$ tuned series indicates that the duration of the MEI is 600 k.y., and is shorter than the same interval recorded in other PTB sections. This is, at least in part, because the PTB bed (Bed 27) is highly condensed and may contain hiatuses from submarine erosion and/or dissolution (Isozaki, 1997; Metcalfe et al., 2001; Nicoll et al., 2002; Payne and Kump, 2007), which resulted in loss of part of the astronomical signal.

3. Huangzhishan (HZS), Zhejing Province, China

Location and facies description. At HZS, located at 30º 55'18.9" N and 119º 59' 21.1" E, 40 km from Meishan, in Zhejing Province, China, the PTB interval is comprised of light-grey, cyclic (1-10 cm) limestone beds with a rich benthic fossil assemblage, deposited in a low-energy shallow marine environment in the lower part of the section, and grey-greenish to black alternating calcareous mudstone and muddy limestone in an inter-platform basin setting with anoxic conditions in the upper part of the section (Chen et al., 2009). High-resolution (2 cm, re-sampled to 1 cm for spectral analysis) MS data (collected for this study) from the section show clear cm to m-scale lithological rhythms (Fig. DR4C); the $\delta^{13}C$ pattern is similar to that at Meishan.

Stratigraphic framework. At HZS, ME_{start} is placed at the base of the *N. meishanensis* zone (base of Bed 19), which is equivalent with *H. latidentatus preparvus–N. meishanensis* zone at Meishan. The *H. parvus* zone starts at the base of Bed 25 and extends to Bed 30, which is equivalent to Meishan Beds 27c-d (*H. parvus* zone). No conodonts have been found in Beds 31-34 at HZS; ME_{end} is placed at the base of Bed 31 (black clay bed), which correlates to the base of Meishan Bed 28 (Chen et al., 2009) (Fig. 1C).

4. Heping (HP), Guizhou Province, China

Location and facies description. The Heping (HP) section is located at 25º 31' N and 106º 31' E in the Nanpanjiang Basin, Guizhou Province, China. Here, the PTB interval consists of ~14 m-thick microbialite which was deposited in a shallow platform environment (Krull et al., 2004). $\delta^{13}C_{org}$ data (Krull et al., 2004) were originally sampled at 2 to 94 cm intervals (averaging 22 cm), here resampled to a uniform 1 cm for time series analysis (Fig. DR4D).

Stratigraphic framework. At HP, ME_{start} occurs at 12.6 m, the contact between the skeletal packstone of the Wujaping Formation and the overlying calcimicrobial framestone, which is also called the "PTB event horizon" (Krull et al., 2004; Lehrmann et al., 2003). This extinction horizon correlates to the base of Meishan Bed 25. The FO of *H. parvus* occurs within the basal 65 cm of the calcimicrobial framestone at HP, which correlates to the base of Bed 27c at Meishan. The *H. latidentatus* zone is defined between the calcimicrobial framestone and the FO of *H. parvus* at Taiping, which is lithologically equivalent with the HP section (Lehrmann et al., 2003). ME_{end} occurs at the FO of *I. isarcica* at 26.7 m at HP (Fig. 1D).

Additional notes on chronology. At HP, the $ME_{\mathbf{start}}$ occurs at the base of the calcimicrobial framestone (CF) unit, which shows evidence for dissolution, and is marked by a sharp negative shift in $\delta^{13}C_{carb}$ (Krull et al., 2004). Correlation of conodont zones and $\delta^{13}C_{carb}$ excursions can be used to estimate the duration between ME1 and ME2 (12.6-26.7 m) (Fig. 1) which represents a 100-k.y. tuned duration of 630 k.y. (Fig. 3D), somewhat shorter than the estimate of 1300 k.y. by (Lehrmann et al., 2003).

5. Gartnerkofel-1 core (GK), Carnic Alps, Austria

Location and facies description. The Gartnerkofel-1 (GK) core is located at 46º 34' 2" N and 13º 17' 58" E, Carnic Alps of Austria has a PTB succession that is ~48 m thick, consisting of cyclic (~20–30 cm) dolomitic limestone interbedded with marls and shales, from a shallow-marine environment (Holser et al., 1989; Rampino et al., 2000). Within the PTB interval, $\delta^{13}C_{carb}$ (Holser et al., 1991) was measured with a 3 cm to 3.17 m sample spacing (averaging 30 cm, resampled to 2 cm in this study) (Fig. DR4E).

Stratigraphic framework. At GK, ME_{start} is at the base of the *H. latidentatus* zone (i.e., the base of the Tesero Horizon, at 231 m); the *H. parvus* zone is from 187.2 m to 224.97 m, and FO of *I. isarcica* is in the interval 188.2-188.6 m, and LO *I. isarcica* in the interval 184.5–185 m, i.e., at the most negative values of $\delta^{13}C$ (Holser et al., 1991; Schönlaub, 1991). Thus, ME_{end} should be in the 188.2-188.6 m interval (start of *I. isarcica*). However, comparing the GK $\delta^{13}C$ pattern with that at Meishan, ME_{start} could be at 224.97 m and ME_{end} could occur as high as 182 m (Fig. 1E).

Additional notes on chronology. At GK, the 100-k.y. tuned MEI duration is 700 k.y. based on correlation of conodont zones (between 230.5 m and 188.2 m) (Schönlaub, 1991), close to the 500 k.y. estimate of (Rampino et al., 2000). Alternatively, matching GK carbon isotope excursions with their counterparts at Meishan, and HP, ME1 and ME2 should be placed at 226 m and 181 m, which also indicates a 700 k.y. duration (Fig. 1E and 3E).

Table DR1 U-Pb ages from Mundil et al. (Mundil et al., 2004) and adjusted U-Pb ages

Sample number	Stratigraphic position (cm)	Mundil et al. 2004 (Ma)	Renne et al., 2010-best fit ages (Ma)	Adjusted U-Pb ages based on 405-k.y. tuned (Ma)
SH32	-313.00	252.50 ± 0.2		
SH10	22.00	252.20 ± 0.4	252.33	252.33
SH09	57.00	252.50 ± 0.3	252.71	252.46
SH27	317.00	253.20 ± 0.3	253.21	253.42

References

Bowring, S. A., Erwin, D. H., Jin, Y. G., Martin, M. W., Davidek, K., and Wang, W., 1998, U/Pb zircon geochronology and tempo of the end-Permian mass extinction: Science, v. 280, no. 5366, p. 1039-1045.

Cao, C. Q., and Shang, Q. H., 1998, Microstratigraphy of Permo-Triassic transitional sequence of the Meishan section, Zhejiang, China: Palaeoworld, v. 9, p. 147-152.

Cao, C. Q., and Zheng, Q., 2009, Geological event sequences of the Permian-Triassic transition recorded in the microfacies in Meishan section: Science in China Series D: Earth Sciences, v. 52, no. 10, p. 1529-1536.

Chen, Z. Q., Tong, J., Zhang, K., Yang, H., Liao, Z., Song, H., and Chen, J., 2009, Environmental and biotic turnover across the Permian-Triassic boundary on a shallow carbonate platform in western Zhejiang, South China: Australian Journal of Earth Sciences, v. 56, no. 6, p. 775-797.

Erwin, D. H., 2006, Dates and Rates: Temporal Resolution in the Deep Time Stratigraphic Record: Annual Review of Earth and Planetary Sciences, v. 34, p. 569-590.

Glen, J. M. G., Nomade, S., Lyons, J. J., Metcalfe, I., Mundil, R., and Renne, P. R., 2009, Magnetostratigraphic correlations of Permian–Triassic marine-to-terrestrial sections from China Journal of Asian Earth Sciences, v. 36, no. 6, p. 521-540.

Hansen, H. J., Lojen, S., Toft, P., Dolence, T., Tong, J., and Michaelsen, P., 2000, Magnetic susceptibility and organic carbon isotopes of sediments across some marine and terrestrial Permo-Triassic boundaries, *in* Yin, H., Dickins, J. M., R., S. G., and Tong, J., eds., Permian-Triassic Evolution of Tethys and Western Circum Pacific: Amsterdam, Elsevier, p. 271-289.

Heller, F., Lowrie, W., Li, H., and Wang, J., 1988, Magnetostratigraphy of the Permo-Triassic boundary section at Shangsi (Guangyuan, Sichuan Province, China): Earth and Planetary Science Letters, v. 88, p. 348-356.

Holser, W. T., Schönlaub, H.-P., Boeckelmann, K., Magaritz, M., and Orth, C. J., 1991, The Permian-Triassic of the Gartnerkofel-1 core (Carnic Alps, Austria): synthesis and conclusions: Abhandlungen der Geologischen Bundesanstalt, v. 45, p. 213-235.

Holser, W. T., Schönlaub, H. P., Attrep Jr, M., Boeckelmann, K., Klein, P., Magaritz, M., Pak, E., Schramm, J.-M., Stattgegger, K., and Schmöller, R., 1989, A unique geochemical record at the Permian/Triassic boundary: Nature, v. 337, p. 39-44.

Isozaki, K., 1997, Permo-Triassic Boundary Superanoxia and Stratified Superocean: Records from Lost Deep Sea: Science, v. 276, no. 5310, p. 235-238.

Jiang, H., Lai, X., Luo, G., Aldridge, R., Zhang, K., and Wignall, P. B., 2007, Restudy of conodont zonation and evolution across the P/T boundary at Meishan section, Changxing, Zhejiang, China: Global and Planetary Change, v. 55, p. 39-55.

Jin, Y. G., Wang, Y., Wang, W., Shang, Q. H., Cao, C. Q., and Erwin, D. H., 2000, Pattern of Marine Mass Extinction Near the Permian-Triassic Boundary in South China: Science, v. 289, no. 5478, p. 432-436.

Kaiho, K., Chen, Z. Q., Kawahata, H., Kajiwara, Y., and Sato, H., 2006, Close-up of the end-Permian mass extinction horizon recorded in the Meishan section, South China: Sedimentary, elemental, and biotic characterization and a negative shift of sulfate sulfur isotope ratio: Palaeogeography, Palaeoclimatology, Palaeoecology, v. 239, p. 396-405.

Kaiho, K., Kajiwara, Y., Nakano, T., Miura, Y., Kawahata, H., Tazaki, K., Ueshima, M., Chen, Z., and Shi, G. R., 2001, End-Permian catastrophe by a bolide impact: evidence of a gigantic release of sulfur from the mantle: Geology, v. 29, p. 815-818.

Krull, E. S., Lehrmann, D. J., Druke, D., Kessel, B., Yu, Y., and Li, R., 2004, Stable carbon isotope stratigraphy across the Permian-Triassic boundary in shallow marine carbonate platforms, Nanpanjiang Basin, South China: Palaeogeography, Palaeoclimatology, Palaeoecology, v. 204, p. 297-315.

Lai, X., Yang, F., Hallam, A., and Wignall, P. B., 1996, The Shangsi section, candidate of the Global Stratotype Section and Point of the Permian-Triassic Boundary, *in* Yin, H., ed., The Palaeozoic-Mesozoic Boundary candidates of Global Stratotype Section and Point of the Permian-Triassic Boundary: Wuhan, China University of Geosciences Press, p. 113-124.

Lean, C. M. B., and McCave, I. N., 1998, Glacial to interglacial mineral magnetic and palaeoceanographic changes at Chatham Rise, SW Pacific Ocean: Earth and Planetary Science Letters, v. 163, p. 247-260.

Lehrmann, D. J., Payne, J. L., Felix, S., Dillett, P. M., Wang, H., Yu, Y., and Wei, J., 2003, Permian-Triassic boundary sections from shallow-marine carbonate platforms of the Nanpanjiang Basin, south China: Implications for Oceanic Conditions Associated with the End-Permian Extinction and Its Aftermath: Palaios, v. 18, no. 2, p. 138-152.

Li, Z., Zhan, L., Zhu, X., Zhang, J., Jin, R., Liu, G., Sheng, H., Shen, G., Dai, J., Huang, H., Xie, L., and Yan, Z., 1986, Mass extinction and geological events between palaeozoic and Mesozoic Era: Acta Geologica Sinca, v. 60, p. 1-17.

Metcalfe, I., Nicoll, R. S., Mundil, R., Foster, C., Glen, J., Lyons, J., Wang, X. F., Wang, C. Y., Renne, P. R., Black, L., Xun, Q., and Mao, X. D., 2001, The Permian–Triassic boundary and mass extinction in China: Episodes, v. 24, no. 4, p. 239-244.

Metcalfe, I., Nicoll, R. S., and Wardlaw, B. R., 2007, Conodont index fossil *Hindeodus changxingensis* Wang fingers greatest mass extinction event: Palaeoworld, v. 16, p. 202-207.

Mundil, R., Ludwig, K. R., Metcalfe, I., and Renne, P. R., 2004, Age and timing of the Permian mass extinctions: U/Pb dating of closed-system zircons: Science, v. 305, no. 5691, p. 1760-1763.

Mundil, R., Metcalfe, I., Ludwig, K. R., Renne, P. R., Oberli, F., and Nicoll, R. S., 2001, Timing of the Permian–Triassic biotic crisis: implications from new zircon U/Pb age data (and their limitations): Earth and Planetary Science Letters, v. 187, no. 1-2, p. 131-145.

Nicoll, R. S., Metcalfe, I., and Wang, C. Y., 2002, New species of the conodont Genus Hindeodus and the conodont boistratigraphy of the Permian-Triassic boundary interval: Journal of Asian Earth Sciences, v. 20, no. 6, p. 609-631.

Payne, J. L., and Kump, L. R., 2007, Evidence for recurrent Early Triassic massive volcanism from quantitative interpretation of carbon isotope fluctuations Earth and Planetary Science Letters, v. 256, no. 1-2, p. 264-277.

Rampino, M. R., Prokoph, A., and Adler, A., 2000, Tempo of the end-Permian event: high-resolution cyclostratigraphy at the Permian–Triassic boundary: Geology, v. 28, p. 643-646.

Schönlaub, H. P., 1991, The Permian–Triassic of the Gartnerkofel-1core (Carnic alps, Austria): conodont biostratigraphy: Abhandlungen der Geologischen Bundesanstalt, v. 45, p. 79-98.

Song, H., Tong, J., and Chen, Z. Q., 2009, Two episodes of foraminiferal extinction near the Permian-Triassic boundary at the Meishan section, South China: Australian Journal of Earth Sciences, v. 56, p. 765-773.

Steiner, M., Ogg, J., Zhang, Z., and Sun, S., 1989, The Late Permian/Early Triassic magnetic polarity time scale and plate motions of South China: Journal of Geophysical Research B: Solid Earth and Planets, v. 94, no. 6, p. 7343-7363.

Wignall, P. B., Hallam, A., Lai, X., and Yang, F., 1995, Palaeoenvironmental changes across the Permian-Triassic boundary at Shangsi (N. Sichuan, China): Historical Biology, v. 10, p. 175-189.

Xie, S., Pancost, R. D., Yin, H., Wang, H., and Evershed, R. P., 2005, Two episodes of microbial change coupled with Permo/Triassic faunal mass extinction: Nature, v. 434, p. 494-497.

Yin, H., Feng, Q., Lai, X., Baud, A., and Tong, J., 2007, The protracted Permo-Triassic crisis and multi-episode extinction around the Permian–Triassic boundary: Global and Planetary Change, v. 55, p. 1-20.

Yin, H., Zhang, K., Tong, J., Yang, Z., and Wu, S., 2001, The global stratotype section and point (GSSP) of the Permian–Triassic boundary: Episodes, v. 24, no. 2, p. 102-114.

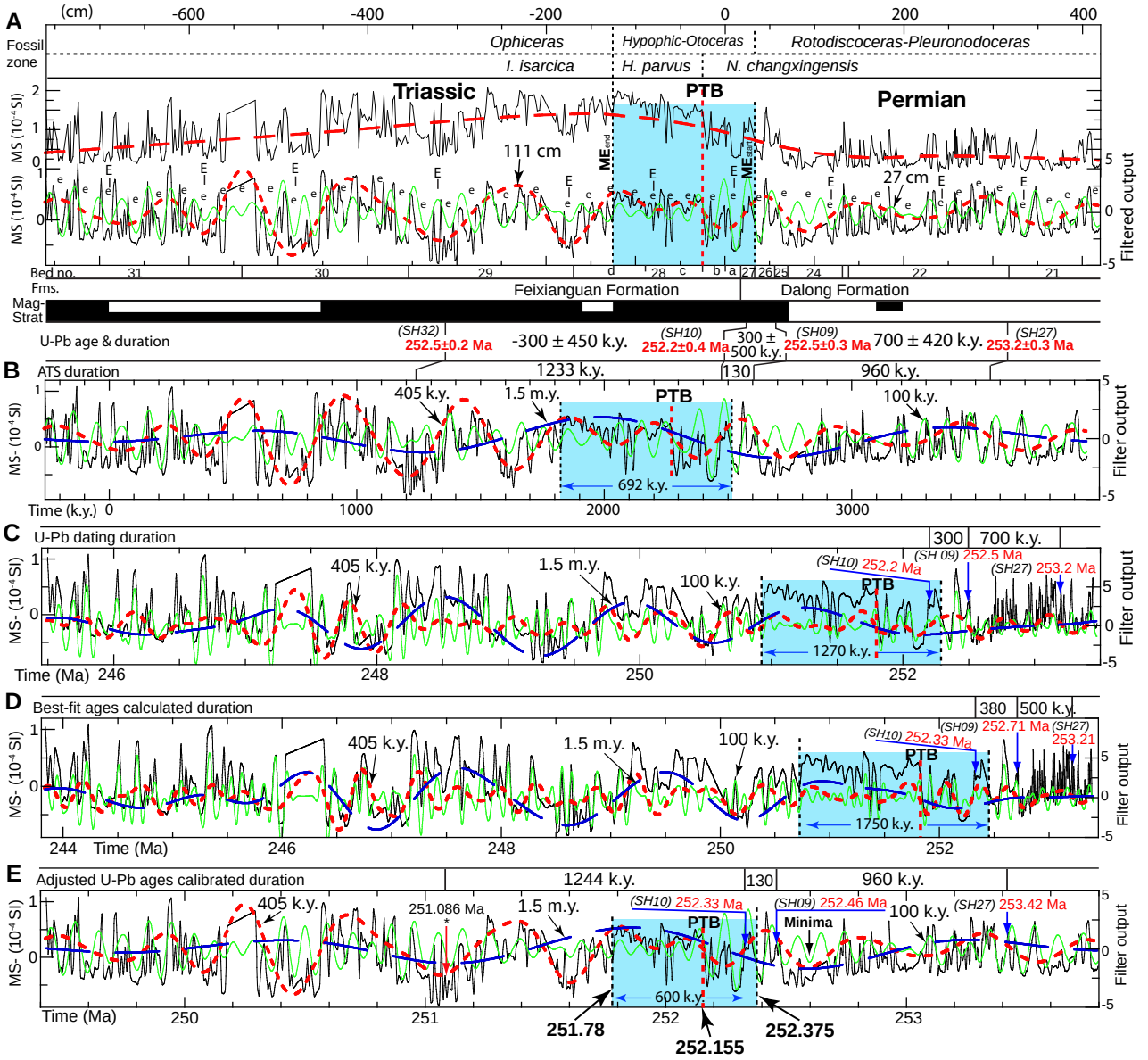

Figure DR1. 405-k.y. astronomical tuning of the Shangsi section MS data across the PTB interval compared with U-Pb age tuning. Shading area indicates the PTB MEI. (**A**) At top, the raw MS series with a 35% weighted average fit curve (red dashed curve); at bottom the MS series after subtracting the 35% weighted average; bandpass filtered ~27 cm cycles (green line) and ~111 cm cycles (red dashed line) from MS represent significant peaks in Fig. 3 which were extracted using Gaussian filters with passbands of 0.009 ± 0.005 per cm and 0.037 ± 0.02 per cm, respectively; MS data from (Hansen et al., 2000); Bed numbers, fossil zones and Fms. (Formation Members) from (Li et al., 1986; Wignall et al., 1995); Magnetic stratigraphy from (Glen et al., 2009); U-Pb ages from (Mundil et al., 2004) and calculated durations from these ages (uncertainties using error propagation). (**B**) 405-k.y. tuned series with 100 k.y. (green line), 405 k.y. (red dashed line) and 1.5 m.y. (blue dashed line) bandpass filters; calculated durations (ATS) based on 405-k.y. tuning. (**C**) SH27, SH09 and SH10 U-Pb age (Mundil et al., 2004) tuned series with 100 k.y., 405-k.y. and 1.5 m.y. filters. (**D**) Renne best-fit ages for SH27, SH09 and SH10 (Renne et al., 2010) tuned series with filters. (**E**) Adjusted U-Pb ages (based on 405-k.y. tuned result) tuned series with short and long eccentricity filter and marked with important event ages. The 100 k.y., 405-k.y. and 1.5 m.y. cycles were extracted using Gaussian filters with a passbands of 0.01 ± 0.005 per k.y., 0.00245 ± 0.0012 per k.y. and 0.00066 ± 0.0004 per k.y., respectively.

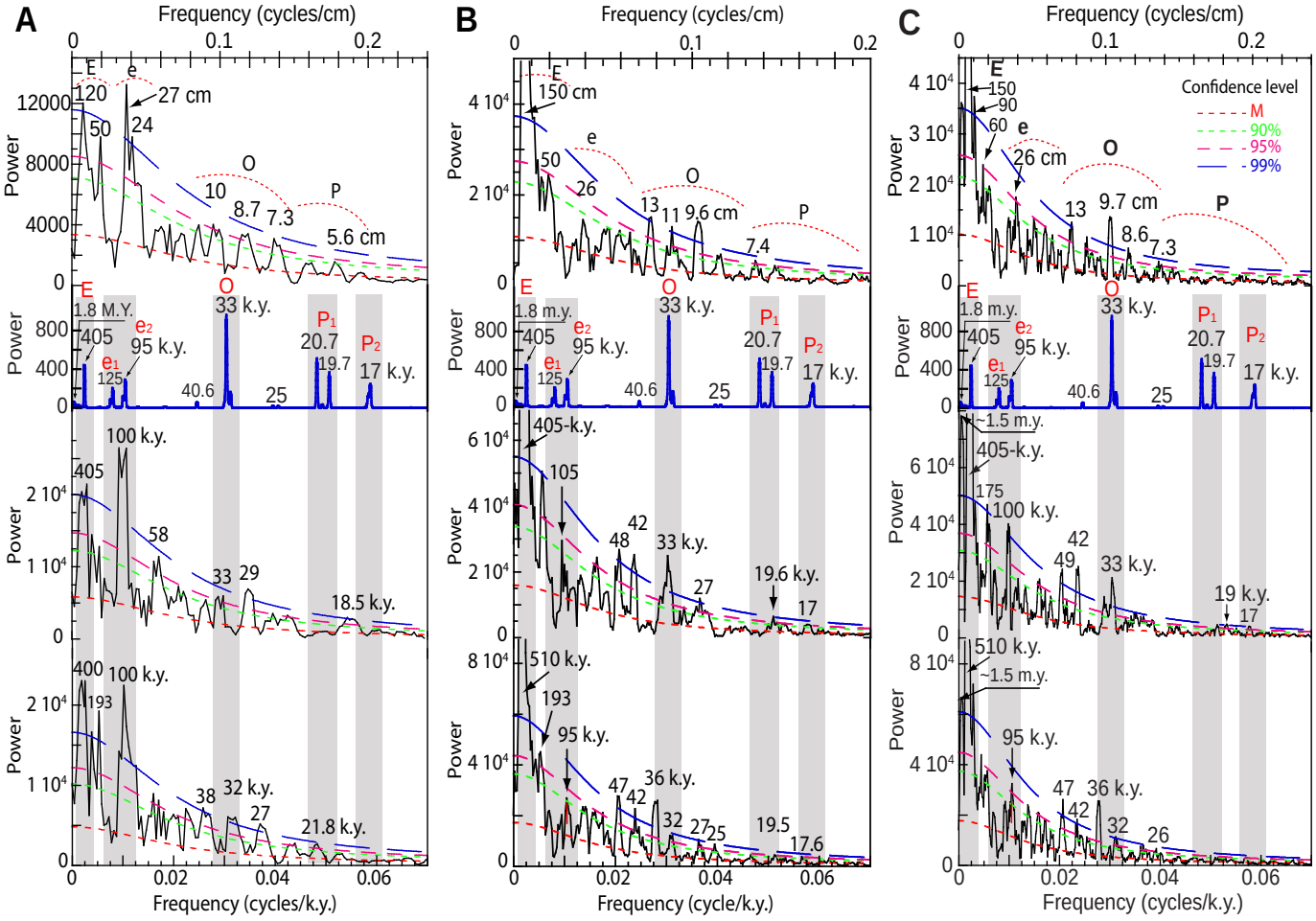

Figure DR2. Spectral analysis using 2π multitapers (MTM) and robust red noise modeling of the untuned and tuned Shangsi MS series. (**A**) From up to down, power spectra of untuned series, the ETP (Earth's astronomical parameters from 240-249 Ma in (standardized) format from the La2004 model (Laskar et al., 2004)), 405-k.y. tuned series and the three adjusted U-Pb ages tuned series for Permian -segment. (**B**) From up to down, power spectra of untuned series, the ETP, 405-k.y. tuned series and the three adjusted U-Pb ages tuned series for Triassic-segment. (**C**) From up to down, power spectra of untuned series, the ETP, 405-k.y. tuned series and the three adjusted U-Pb ages tuned series for entire MS series. Significant peak labeled in cm and k.y..

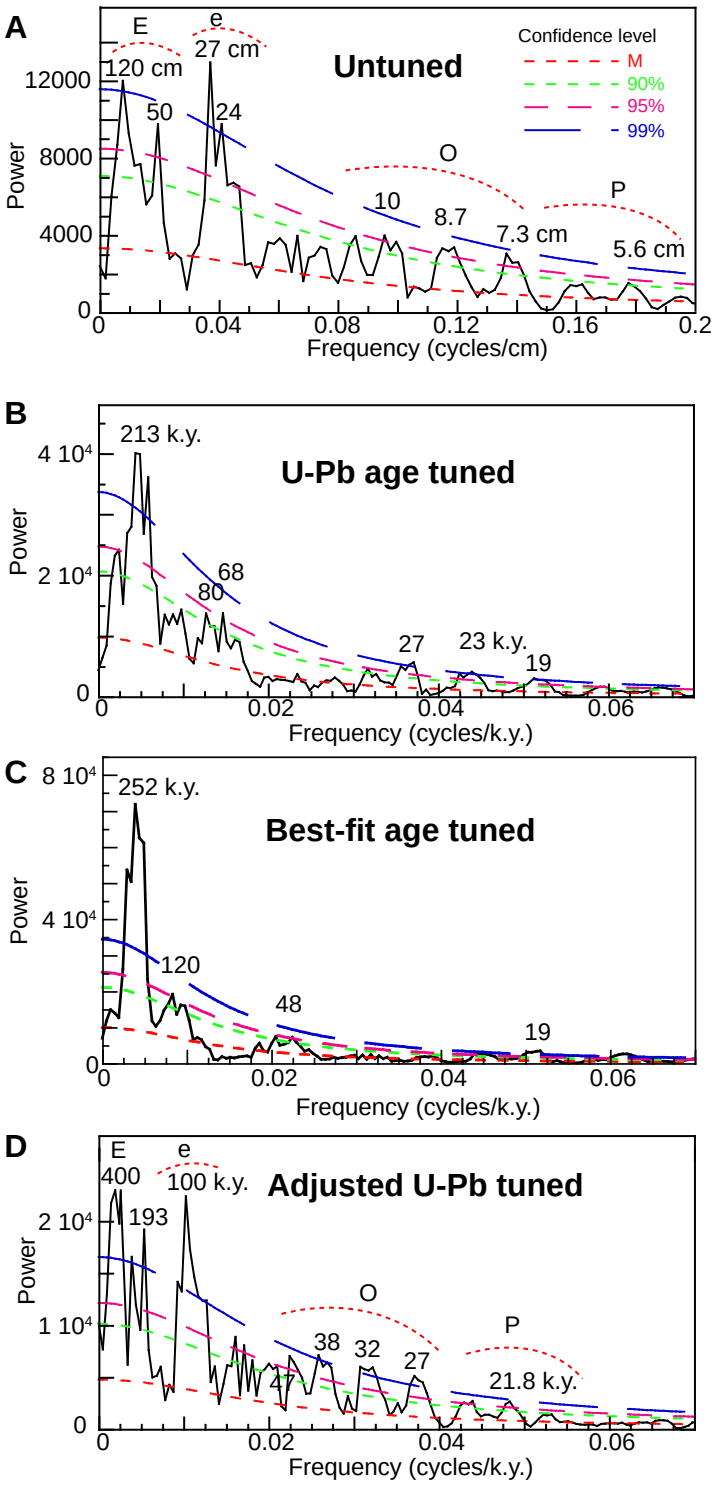

Figure DR3. 2π multitaper (MTM) power spectra of untuned (**A**), U-Pb age tuned (**B**), Best -fit age tuned (**C**) and adjusted U-Pb tuned (**D**) MS series with robust red noise models (using the SSA-MTM Toolkit) from the Permian part of the Shangsi section.

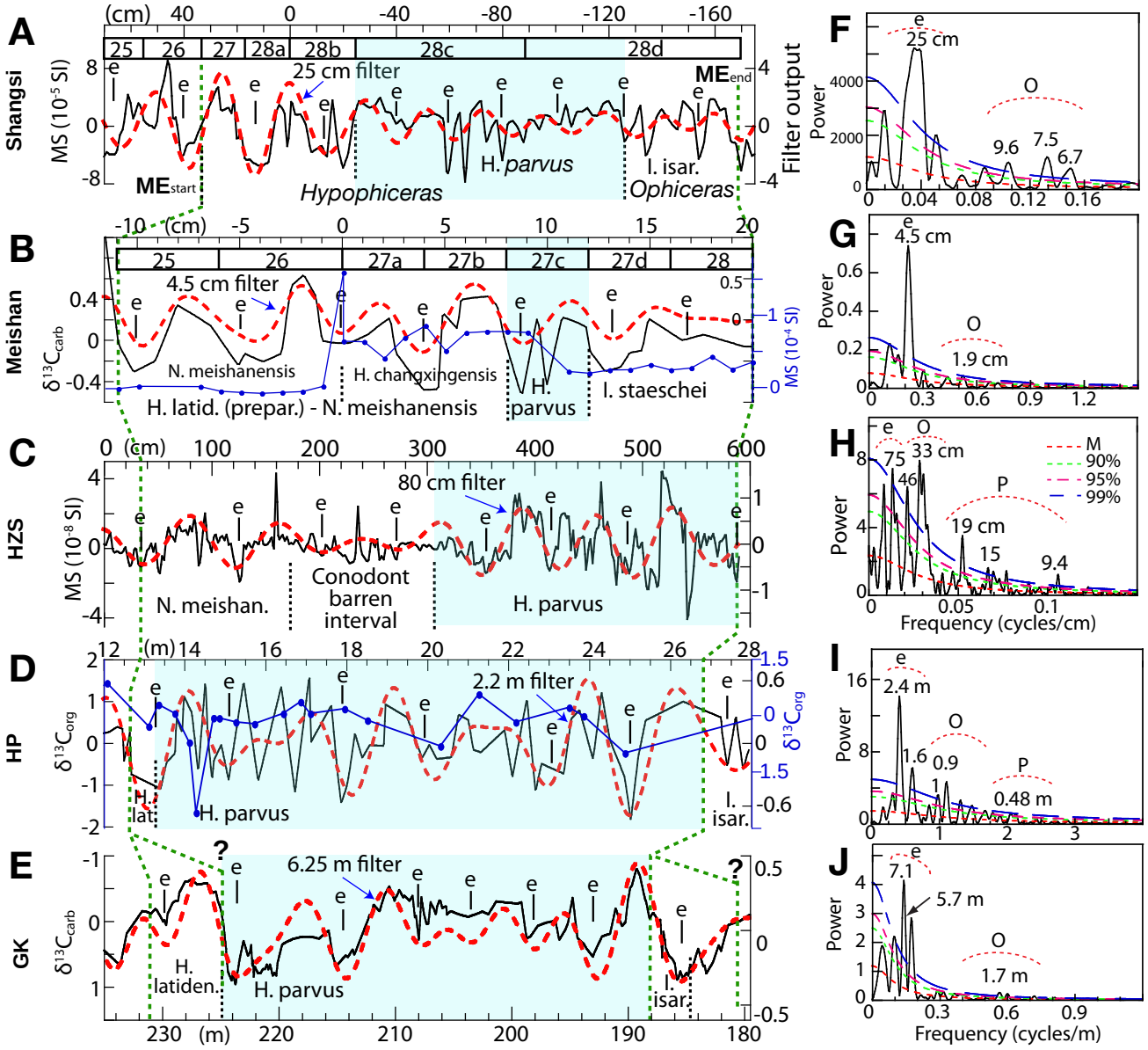

Figure DR4 Untuned series of the PTB MEI data (black curves, left side) with Gaussian bandpass filtered output (red dashed curves) and 2π multitaper (MTM) spectral analysis (black curves, right side) using AnalySeries 2.0.4.2 and the SSA-MTM Toolkit. Light blue shaded areas indicate the *H. parvus* zone. (**A**) Shangsi MS series with 25 cm filter (passband: 0.04 ± 0.012 cycle/cm); (**B**) Meishan B $\delta^{13}C_{carb}$ series with 4.5 cm filter (passband: 0.22 ± 0.1 cycles/cm); Blue curve is the MS; (**C**) HZS MS series with 80 cm filter (passband: 0.0125 ± 0.004 cycles/cm); (**D**) HP $\delta^{13}C_{org}$ series with 2.2 m filter (passband: 0.45 ± 0.2 cycles/m); Blue curve is the $\delta^{13}C_{carb}$; (**E**) GK $\delta^{13}C_{carb}$ series with 6.25 m filter (passband: 0.16 ± 0.1 cycles/m). **F-J** are the power spectra of the untuned series to the left, compared to robust red noise models.